energies

MDPI

Article

Numerical Study on the Characteristics of Hydrogen Leakage, Diffusion and Ventilation in Ships

Chang-Yong Lee [1] and Sang-Kyun Park [2,*]

[1] Department of Maritime Police & Technology, Gangwon State University, Gangneung 25425, Republic of Korea; cylee@gw.ac.kr
[2] Division of Maritime AI & Cyber Security, National Korea Maritime and Ocean University, Busan 49112, Republic of Korea
* Correspondence: skpark@kmou.ac.kr; Tel.: +82-51-410-4579

Abstract: Hydrogen is a promising environmentally friendly fuel with the potential for zero-carbon emissions, particularly in maritime applications. However, owing to its wide flammability range (4–75%), significant safety concerns persist. In confined spaces, hydrogen leaks can lead to explosions, posing a risk to both lives and assets. This study conducts a numerical analysis to investigate hydrogen flow within hydrogen storage rooms aboard ships, with the goal of developing efficient ventilation strategies. Through simulations performed using ANSYS-CFX, this research evaluates hydrogen diffusion, stratification, and ventilation performance. A vertex angle of 120° at the ceiling demonstrated superior ventilation efficiency compared to that at 177°, while air inlets positioned on side-wall floors or mid-sections proved more effective than those located near the ceiling. The most efficient ventilation occurred at a velocity of 1.82 m/s, achieving 20 air exchanges per hour. These findings provide valuable insights for the design of safer hydrogen vessel operations.

Keywords: hydrogen diffusion; hydrogen leakage; ventilation; shipboard hydrogen storage; computational fluid dynamics; ceiling apex angle

check for updates

Academic Editor: Erik Kjeang

Received: 25 November 2024
Revised: 13 January 2025
Accepted: 17 January 2025
Published: 20 January 2025

Citation: Lee, C.-Y.; Park, S.-K. Numerical Study on the Characteristics of Hydrogen Leakage, Diffusion and Ventilation in Ships. *Energies* **2025**, *18*, 448. https://doi.org/10.3390/en18020448

Copyright: © 2025 by the authors. Licensee MDPI, Basel, Switzerland. This article is an open access article distributed under the terms and conditions of the Creative Commons Attribution (CC BY) license (https://creativecommons.org/licenses/by/4.0/).

1. Introduction

The advancement of industrial technologies and expansion of the global economy have led to increased environmental pollution and global warming. In particular, the emission of greenhouse gases (GHGs) from fossil fuel consumption is accelerating climate change. The primary GHGs are carbon dioxide (CO_2), methane (CH_4), and nitrous oxide (N_2O) [1,2]. The Paris Climate Agreement of 2015 established regulations on GHG emissions, the phase-out of fossil fuels, and the increased adoption of renewable energy sources [3]. The international shipping sector accounts for over 90% of global trade and has become a considerable source of GHG emissions, volatile organic compounds, particulate matter (PM), and other atmospheric pollutants. From 2007 to 2012, the maritime industry emitted an annual average of 1.038 billion tons of greenhouse gases [4].

To address these GHG emissions, the International Maritime Organization (IMO) devised an initial strategy aimed at reducing the carbon intensity of the global shipping industry by 40% by 2030 and 70% by 2050 relative to 2008 levels. Additionally, it set a goal to cut total international shipping GHG emissions by more than 50% by 2050 [5]. In 2020, the fourth IMO GHG study reported that shipping-related GHG emissions in 2018 constituted 2.89% of total human-induced CO_2 emissions and projected an increase of 90–130% by 2050 compared to 2008 levels [6]. In response, the IMO's 80th Marine Environment Protection Committee (MEPC) formulated a more ambitious GHG reduction policy for international

shipping through its 2023 GHG strategy revision. This strategy aims to decrease annual international shipping GHG emissions by 20–30% by 2030 and 70–80% by 2040 and achieve net-zero emissions by 2050, all relative to 2008 levels [7].

To meet these objectives, the shipping industry is increasingly investing in the development and application of low-carbon and carbon-neutral marine fuels. While low-carbon substitutes can address current IMO environmental standards, carbon-neutral fuels are expected to dominate the market for ship fuel alternatives in the future [8]. Shipowners are considering several alternative fuel options, including liquefied natural gas (LNG), biodiesel, liquefied biogas, ammonia, methanol, battery and electric power, and hydrogen. Among these, LNG has been the most prevalent alternative fuel in recent years [9–11]. However, given its fossil fuel origin, LNG is viewed as a temporary solution for reducing CO_2 emissions in current maritime operations rather than a long-term alternative fuel [12,13].

Currently, ammonia and hydrogen, the most commercially viable carbon-neutral fuels, are gaining attention as alternative fuels capable of achieving decarbonization in the shipping industry [14]. Ammonia is considered promising owing to its composition of only hydrogen and nitrogen, which means it lacks carbon and sulfur, resulting in carbon-free combustion. However, propulsion systems utilizing ammonia fuel are 20–60% more costly than conventional vessels, leading to the consideration of ammonia fuel cells as a more practical alternative [15,16]. On the downside, ammonia's toxicity is triple that of methanol or gasoline, and it has a low flash point. Furthermore, before its adoption as a marine fuel, further research is required on safety protocols, environmental impact evaluations, and economic viability [17–20].

Hydrogen is viewed as the most promising alternative fuel, producing zero pollutants during combustion. It possesses a low minimum ignition energy of 0.02 mJ, a broad combustion range of 4–75.6%, and a flame velocity of 270 cm/s, which surpasses LNG (38 cm/s) by 7.1 times, methanol (50 cm/s) by 5.4 times, and liquid ammonia (14 cm/s) by 19.2 times [21,22]. However, hydrogen has the smallest molecular volume. Therefore, its embrittlement, which causes it to diffuse easily into steel and other metals, can reduce material strength, making structures prone to failure. While minor hydrogen leaks tend to dissipate rapidly, major leaks can generate jets that, under the influence of buoyancy, may form hydrogen–air mixtures, increasing the risk of jet fires and explosions [23]. The hydrogen accident analysis database, supported by the U.S. Department of Energy, reveals that between 1999 and 2019, 57.9% of 120 total accidents occurred in research facilities, hydrogen fueling stations, and hydrogen-related commercial installations. Moreover, 60.5% of accidents were associated with components such as piping, fittings, valves, storage units, fuel cell vehicles, and fuel distribution systems [23,24]. These accidents can lead to catastrophic outcomes, as sudden leaks in open or enclosed spaces can quickly transition from deflagration to detonation due to the highly reactive nature of hydrogen, necessitating immediate intervention [25–27].

To safely and efficiently utilize hydrogen as a clean energy source, it is crucial to thoroughly understand its safety aspects. Globally, extensive research on hydrogen leakage and diffusion is being conducted through both experimental studies and computational fluid dynamics (CFD) techniques to assess potential hazards [28,29]. Experimental studies on hydrogen leak behavior have been largely confined to scaled models or controlled environments owing to safety concerns, high risks, and associated costs [30–35]. Consequently, CFD simulations have become the primary tool for investigating hydrogen leakage and diffusion patterns [36–40]. Conducting hydrogen leak experiments in confined spaces, such as those aboard ships, poses considerable risks. Therefore, most studies on potential hydrogen leak scenarios in hydrogen-powered vessels are carried out through CFD simulations, providing valuable insights into the mechanisms of hydrogen leakage and diffusion.

Li et al. [41] used Ansys Fluent software to examine the distribution of hydrogen concentrations within cabins under various ventilation scenarios and proposed recommendations for sensor placement and ventilation parameters. Similarly, Gao et al. [42] employed Ansys Fluent to model hydrogen diffusion following hydrogen fuel cell vehicle leaks aboard carrier vessels, analyzing the effects of leak locations and ventilation on hydrogen concentration and spread. Mao et al. [43] conducted simulations of hydrogen diffusion across multiple sections of hydrogen fuel cell ships, including fuel cell chambers, control centers, and passenger compartments, analyzing temporal changes in hydrogen concentration patterns. Xie and collaborators [44] simulated hydrogen leakage and diffusion within ship engine compartments, investigating how ventilation conditions, leak quantities, and temperature influence these processes. Kim and Hwang [45,46] assessed how the motion amplitudes of ships affect hydrogen diffusion and ventilation flow rates in the confined spaces of hydrogen-powered vessels equipped with mechanical ventilation. They also proposed ventilation capacity calculations that consider exhaust positioning and the effects of ship motion. Soto et al. [47] analyzed hydrogen release and diffusion from compressed hydrogen storage rooms located beneath ship decks and proposed improvements and mitigation strategies for ventilation systems in enclosed or partially confined spaces.

This study presents a numerical analysis of hydrogen flow and diffusion from hydrogen tank storage rooms installed below ship decks, utilizing ANSYS CFX software (v18.1). To evaluate hydrogen stratification phenomena in relation to ceiling apex angles, the storage room's ceiling apex angles were modeled at 177.7° and 120°. This study examined the flow and diffusion characteristics as functions of hydrogen leak rates, air inlet and ventilation hole (exhaust port) locations, and ventilation velocities.

This study is expected to be applicable to industrial facilities and buildings involved in the production, use, and distribution of hydrogen. In particular, it can provide data necessary for the installation standards of ventilation facilities applicable to H2PEM power plants and hydrogen fuel cell operating facilities that produce electricity.

To date, most research papers on hydrogen leakage have focused on scenarios involving hydrogen refueling stations, power plants, or fuel cell vehicles. Although some studies have addressed hydrogen leakage on ships, this study differs from previous research in that it models the hydrogen tank storage room at a scale comparable to an actual operating vessel, enabling practical applicability. By selecting a ship of appropriate scale as a model for testing before applying the findings to commercial vessels, the results of this study are expected to have significant practical utility.

At present, there is a lack of well-defined legislation, standards, and guidelines pertaining to the use of hydrogen as a ship fuel, as well as a scarcity of internationally standardized technical data. The significance of this study lies in its provision of experimental evidence and foundational design data aimed at preventing safety accidents and establishing safety standards for hydrogen-powered ships. It is anticipated that this research will contribute significantly to the development of safety risk assessment criteria for hydrogen leak accidents. Moreover, the findings of this study are expected to serve as a crucial technical reference for various ventilation parameters that must be considered when designing effective ventilation systems for hydrogen tanks in confined spaces.

2. CFD Theoretical Fundamentals

2.1. Governing Equations

The diffusion dynamics of hydrogen–air mixtures are governed by equations that encompass momentum, mass, energy, and chemical species [44,47,48].

The continuity equation for the mixture is given by Equation (1):

$$\frac{\partial \rho}{\partial t} + \nabla \cdot (\rho_g \vec{v}) = 0 \quad (1)$$

where ρ_g is gas density (kg/m^3), t is time (s), and $\vec{v}$ is the velocity vector (m/s).

Momentum conservation is given by Equation (2):

$$\frac{\partial}{\partial t}(\rho \vec{v}) + \nabla \cdot (\rho_g \vec{v}\ \vec{v}) = -\nabla p + \nabla \cdot (\tau) + \rho_g \cdot \vec{g} \quad (2)$$

where g is the gravitational acceleration (9.8 m/s^2) and τ is the stress tensor, as given in reference [48].

Energy conservation is expressed by Equation (3):

$$\frac{\partial}{\partial t}(\rho E) + \nabla \cdot (\vec{v}\,(\rho_g E_g + p)) = \nabla \cdot (\lambda_{eff} \nabla T_g - \sum_i h_i J_i + (\tau_{eff} \cdot \vec{v})) \quad (3)$$

where $\lambda_{eff} \nabla T_g$ is the conductive term, $\sum_i h_i J_i$ is the diffusive term associated with the flux of species, $\tau_{eff} \cdot \vec{v}$ incorporates viscous dissipation, E is the total energy in J, λ_{eff} is effective thermal conductivity in (W/(m·K)), ∇T_g is the temperature gradient (K/m), h_i the sensible enthalpy of species i in (J/kg), and J_i is the diffusion flux of species i (kg/m^2·s).

The species transport equation is expressed by Equation (4):

$$\frac{\partial (\rho Y_i)}{\partial t} + \nabla \cdot (\rho_g \vec{v} Y_i) = -\nabla \cdot \vec{J_i} \quad (4)$$

Diffusion mass flux for turbulent flow is given by Equation (5):

$$\vec{J_i} = -(\rho_g D_{i,m} + \frac{\mu_t}{Sc_t}) \nabla Y_i \quad (5)$$

The species transport equation (Equation (4)) depends only on the diffusive mass flux given by Equation (5). This includes Fick's molecular diffusion term $\rho_g D_{i,m}$ and the turbulent term $\frac{\mu_t}{Sc_t}$. Y_i is the mass fraction of species i in (kg/kg), $D_{i,m}$ is the diffusion coefficient in (m^2/s), μ_t is turbulent viscosity (kg/(m·s)), and Sc_t is the turbulent Schmidt number (-).

2.2. Turbulence Model

Hydrogen leakage in confined spaces causes pressure fluctuations. The resulting flow of leaked hydrogen is complex and typically turbulent. This study employs the standard $k-\varepsilon$ model [49] to analyze these turbulent phenomena.

The turbulent kinetic energy *k* equation is represented by Equation (6):

$$\frac{\partial (\rho k)}{\partial t} + \frac{\partial (\rho k u_i)}{\partial x_i} = \frac{\partial}{\partial x_j}\left[(\mu + \frac{\mu_t}{\sigma_k}) \frac{\partial k}{\partial x_i}\right] + G - \rho \varepsilon \quad (6)$$

The turbulent dissipation rate ε equation is given by Equation (7):

$$\frac{\partial (\rho \varepsilon)}{\partial t} + \frac{\partial (\rho \varepsilon u_i)}{\partial x_i} = \frac{\partial}{\partial x_j}\left[(\mu + \frac{\mu_t}{\sigma_\varepsilon}) \frac{\partial \varepsilon}{\partial x_j}\right] + C_{1\varepsilon} G \frac{\varepsilon}{k} + C_{2\varepsilon} \rho \frac{\varepsilon^3}{k} \quad (7)$$

where k represents turbulent kinetic energy (m^2/s^2), ε is the energy dissipation rate (m^2/s^3), G is the generation of turbulent kinetic energy (kg/ms^3), and σ_k,σ_ε,$C_{1\varepsilon}$ and $C_{2\varepsilon}$ are constants. Table 1 presents the constants employed in this turbulence model.

Table 1. Constant values for the standard k − ε turbulence model.

$C_{1\varepsilon}$	$C_{2\varepsilon}$	C_{μ}	σ_k	σ_{ε}
1.44	1.93	0.09	1.0	1.3

3. Numerical Models and Grid Validation

3.1. Physical Model

The subject of this research is a 260-ton class vessel measuring 38 m in length, 8 m in width, and 4.6 m in depth. This vessel, an LNG-powered harbor promotional vessel (E-ship), was selected as the physical model owing to its appropriate scale for empirical validation prior to the commercialization of larger hydrogen-fueled vessels. The ship incorporates an independent, cylindrical LNG storage tank and is equipped with a single air inlet and ventilation exhaust ports. For the purpose of this analysis, the LNG storage tank and its associated room were modeled as a hydrogen tank and storage room, respectively. The dimensions of the hydrogen tank storage room were 5.28 m (width), 8.98 m (length), and 3.8 m (height), with a ceiling vertex angle (A) of 177.7°, as illustrated in Figure 1.

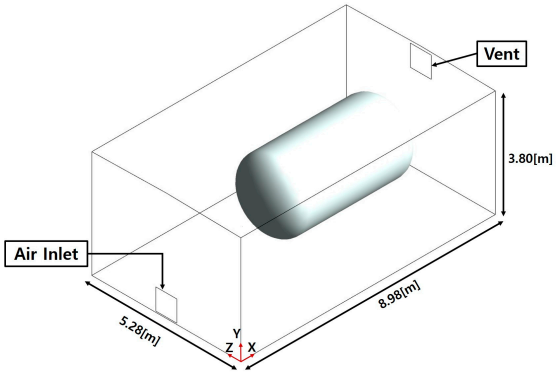


Figure 1. Geometry of the hydrogen tank storage room (A = 177.7°).

The leak orifice diameter was fixed at 20 mm, while the air inlet and ventilation hole dimensions were set at 740 mm × 740 mm. To investigate hydrogen stratification phenomena, various leak rates (1, 2, and 4 g/s), ventilation velocities (0, 1.82, 2.73, 3.64, 4.55, and 5.46 m/s), and ceiling vertex angles (177.7°, 120°) were considered. For other analyses concerning leak rates, air inlet and ventilation hole positions, and ventilation characteristics at different ventilation velocities, a ceiling vertex angle of A = 120° was used. The leak point was positioned at the upper junction between the hydrogen tank's shell and head to examine the flow characteristics of the escaping hydrogen gas. The physical model was constructed using ANSYS CFX software, with the hydrogen tank dimensions set at φ 2.40 m × 4.85 m and the volume at 20 m^3.

3.2. Boundary Conditions

The boundary conditions for the numerical model were as follows:

- The internal temperature of the hydrogen tank storage room was set at 298 K, with an ambient pressure of 101.325 kPa. To account for gravitational and buoyancy effects on hydrogen leak diffusion, gravitational acceleration was defined as −9.81 m/s^2 along the negative *y*-axis.
- The hydrogen tank and storage room walls were designated as no-slip walls, with a turbulence intensity of 5%. The time step was set to 0.001 s, residual target to 10^{-5}, and total simulation time to 600 s.

- Two ventilation systems were implemented: one with a natural air inlet and natural exhaust and another with a natural air inlet and forced exhaust. For the natural air inlet, a gauge pressure of 0 Pa was used, allowing backflow. Forced ventilation velocities corresponding to flow rates of 1800, 3600, 5400, 7200, and 9000 m^3/h were established to evaluate ventilation effectiveness, with backflow excluded.

3.3. Verfication and Validation of CFD Model

A grid independence study was conducted using Fluent Meshing software (v18.1) to optimize the simulation model. Hexahedral grids were used, with refined meshes in the hydrogen leak regions. Three grid densities were tested: 1,491,666 (Grid I), 2,443,214 (Grid II), and 3,892,722 (Grid III). Figure 2 is a graph that tests grid dependence. The height–hydrogen-mole-fraction relationship was analyzed by tracing an imaginary vertical line from the leak source to the storage room ceiling (Figure 2). A 4 g/s leak rate was chosen to maximize mole-fraction variations. The results showed negligible differences between Grid II and Grid III. Figure 3 shows the cross section and leak outlet of a hydrogen storage tank with a completed grid. To optimize calculation time and accuracy, the grid corresponding to Grid II was used to generate the mesh, as shown in Figure 3.

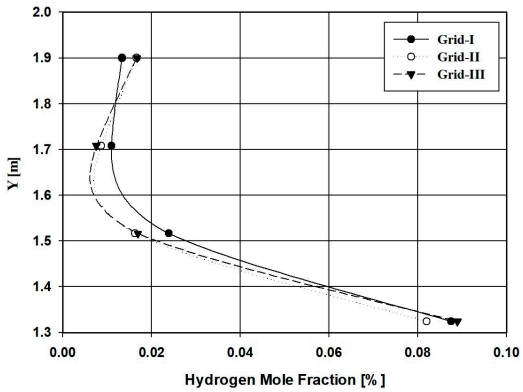


Figure 2. Independence test for grids.

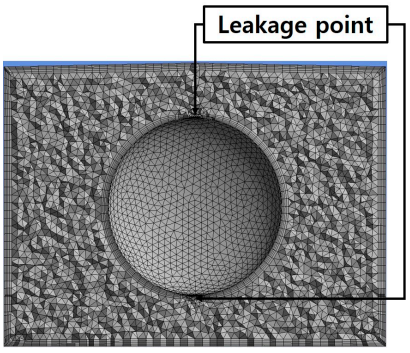


Figure 3. Meshing and leakage points.

The results obtained from the numerical model must be compared with experimental data to verify the accuracy of the simulation. In this study, the experimental results from INERIS [50] were compared with the simulation results obtained using the CFD program Fire Dynamics Simulator (FDS) [51]. The INERIS experimental setup involved a leak orifice with a 20 mm diameter, a hydrogen release rate of 1 g/s, and a leak duration of 240 s. Figure 4 illustrates the measured molar concentrations of leaked hydrogen at positions corresponding to the hydrogen sensors within the chamber. Sen 13 and Sen 14 were located at (0, 0, 2.68) and (0, 0, 2.38) in (x, y, z) coordinates, respectively, which match the sensor positions described in references [50,51]. A comparison with the INERIS experimental data

revealed a maximum temporal deviation of approximately 3%, as shown in Figure 4, while the discrepancy with the numerical analysis results from reference [51] was approximately 4%. Given the negligible differences between experimental and computational results, the numerical analysis presented in this study was deemed reliable.

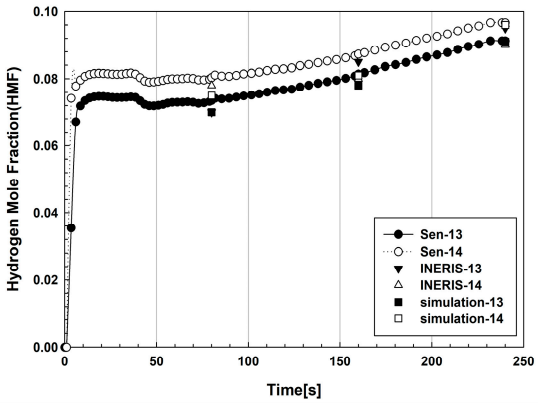


Figure 4. Validity of simulation.

4. Results and Analysis

4.1. Effect of Ceiling Apex Angle on Hydrogen Stratification

Boundary conditions for hydrogen stratification analysis are presented in Table 2.

Table 2. Boundary condition settings.

Item	Boundary Condition
Storage room temperature	298 K
Leak rate	2 g/s
Leak location	Top of the tank
Air inlet and exhaust positions	Inlet 1, Vent 2
Exhaust flow rate	None (natural ventilation condition)

Apex angles (A) of 177.7° and 120° were selected to evaluate the stratification degrees of leaked hydrogen in relation to the ceiling's geometry. Figure 5 shows the shape of the hydrogen tank storage room used in the simulation. Figure 5 illustrates these configurations, with A = 177.7° corresponding to the E-ship's actual ceiling apex angle and A = 120° representing a theoretical angle based on potential hydrogen tank storage room designs in ships.

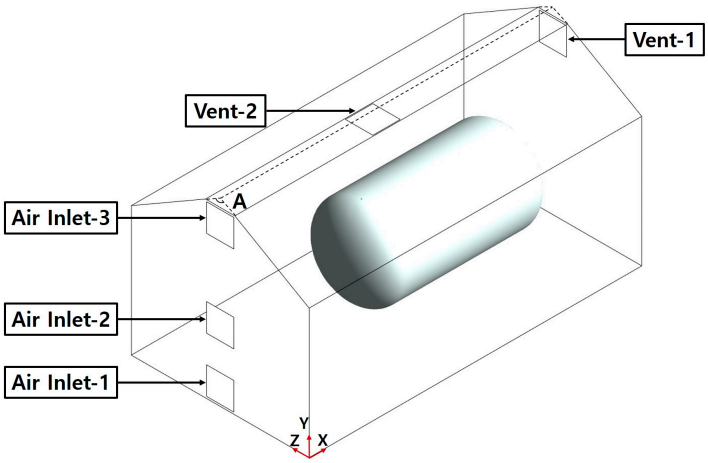


Figure 5. Configuration of the hydrogen tank storage room.

Figure 6 depicts the hydrogen mole fraction over the y = 3.8 m plane, which includes the hydrogen leak point extending to the ceiling under natural air inlet and exhaust conditions. Upon leakage from the tank, hydrogen rapidly formed stratified layers along the ceiling, progressively extending toward the floor. Consistent with the observations in reference [52], three distinct layers were observed: a high-concentration upper layer, medium-concentration middle layer, and low-concentration layer near the floor. Figure 6a formed thicker and more concentrated layers at the ceiling compared to Figure 6b. This confirms the substantial impact of the ceiling apex angle on hydrogen stratification. Particularly, the A = 120° scenario resulted in thinner concentration layers even under natural ventilation, indicating that a steeper ceiling inclination could enhance ventilation efficiency.

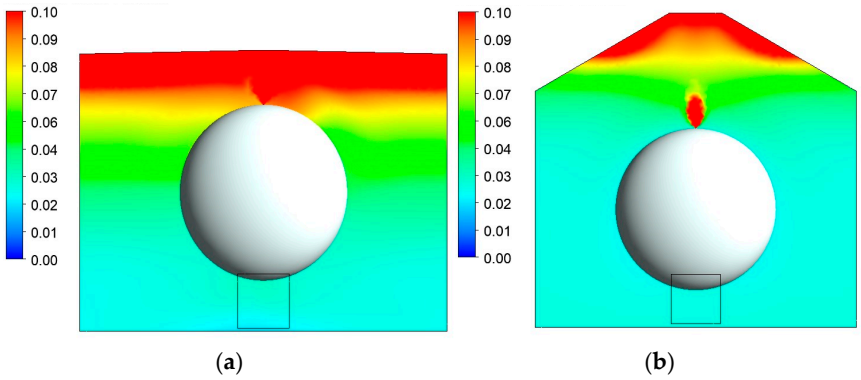


Figure 6. Hydrogen concentration distribution according to ceiling apex angle: (**a**) A = 177.7°, (**b**) A = 120°.

Figure 7 illustrates the temporal and spatial variations in hydrogen concentration at three vertical positions: y = 3.8 m (upper region), y = 1.9 m (middle region), and y = 0.5 m (lower region). As A decreased from 177.7° to 120°, the hydrogen mole fraction reduced from 29.4% at y = 3.8 m to 13.3% at y = 0.5 m. In the near-ceiling regions (y = 3.8 m and y = 1.9 m), hydrogen mole fractions increased sharply during the first 100 s before plateauing, while at y = 0.5 m, a continuous increase was observed for approximately 400 s. Based on these observations, A is shown to be a critical factor influencing the stratification of leaked hydrogen, suggesting that the ceiling apex angle should be carefully considered for effective ventilation under natural air inlet and exhaust conditions.

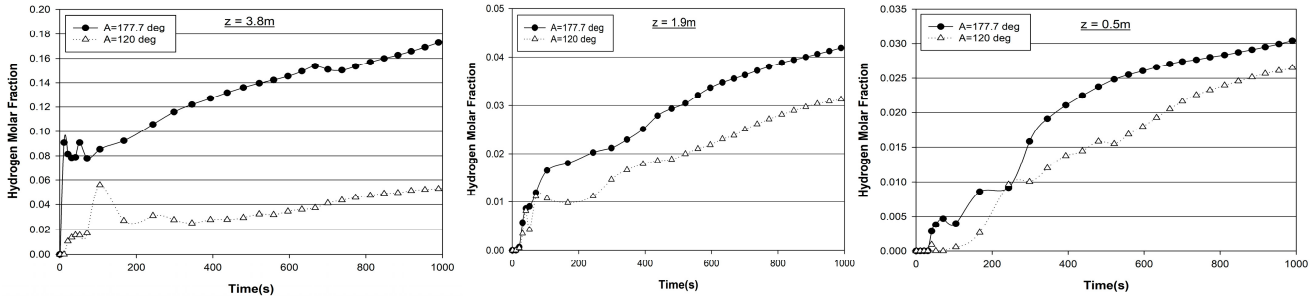


Figure 7. Hydrogen molar fraction for ceiling apex angle (A).

4.2. Effect of Leakage Rate on Hydrogen Diffusion

The Korean Register's "Marine Fuel Cell System Guidelines" (2020) mandate the installation of negative pressure ventilation systems with at least 30 air changes per hour in enclosed spaces such as tank connection areas or fuel preparation rooms.

This study implemented Type III ventilation—natural inlet and forced exhaust—for the hydrogen tank storage room, setting the ventilation velocity to 2.73 m/s to achieve

the required 30 air changes per hour. The calculation time spanned from 0 to 600 s post-hydrogen leak initiation. Three leak rates were investigated, Q_1 (1 g/s), Q_2 (2 g/s), and Q_3 (4 g/s), with fixed parameters including a 20 mm leak orifice diameter, air inlet at Inlet 1, and ventilation hole at Vent 1. The storage room was maintained at a uniform temperature of 298 K. The leak source was positioned at (0, 1.24, 0), corresponding to the upper central point where the tank shell meets the head. Hydrogen diffusion volume was analyzed by measuring the average volume of leaked hydrogen within the storage chamber.

Hydrogen diffusion was shown on the YZ plane (X = 0), with concentration levels ranging from 0 to 0.04. Figure 8 and Table 3 present the temporal evolution of hydrogen diffusion volume and process.

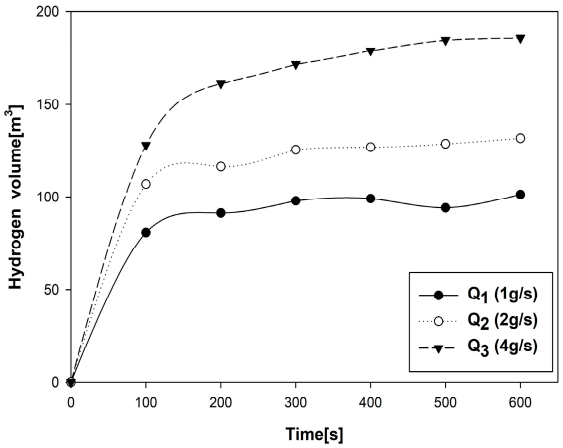
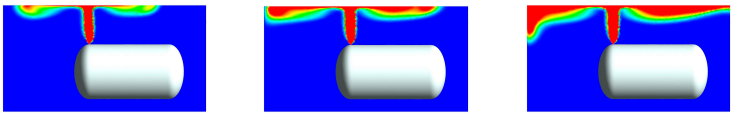
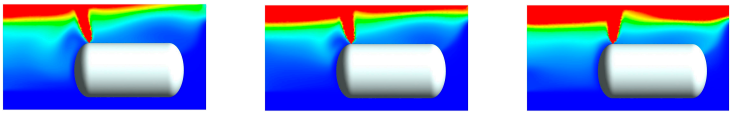
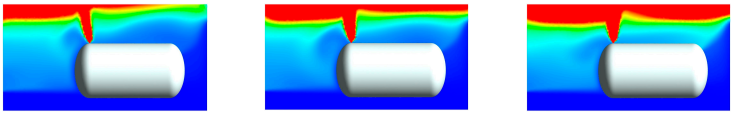
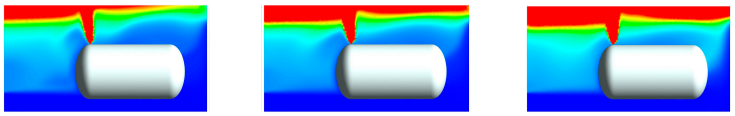
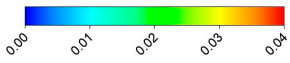


Figure 8. Hydrogen volume over time (diffusion volume of leaked hydrogen over time).

Table 3. Hydrogen diffusion state in hydrogen tank chamber.

Time (s)	Leakage Rate		
	Q_1 (1 g/s)	Q_2 (2 g/s)	Q_3 (4 g/s)
10			
100			
300			
600			
			

As shown in Figure 8, the gas diffusion exhibited rapid expansion during the initial 100 s, transitioning to a more gradual diffusion thereafter. The leak rate of Q3 showed nearly double the diffusion extent of Q1, indicating a positive correlation between leak rate and sustained hydrogen concentration increase within the storage room.

Table 3 shows that for all leak rates—Q1, Q2, and Q3—hydrogen reached the ceiling within 10 s and subsequently diffused symmetrically along the ceiling surface. Despite

the differences in leak rates, the diffusion patterns followed similar trends, with hydrogen impacting the ceiling, flowing along its surface, and stratifying from ceiling to floor. The vertical region above the wall containing the air inlet exhibited a higher concentration of hydrogen compared to the side wall with the ventilation hole. This phenomenon can be attributed to the continuous ventilation currents formed at the ventilation wall, which maintained relatively lower hydrogen concentration layers. Moreover, the air inlet resulted in reduced hydrogen concentrations in the stratified layers near the floor, with similarly low concentrations observed in the airflow path leading to the ventilation hole.

These observations suggest that upon hydrogen leakage, the combined effects of buoyancy and the jet-like discharge from the leak point caused the hydrogen to collide with the walls while rapidly expanding in volume owing to inertial forces. Consequently, to ensure prompt detection of hydrogen leaks, it is advisable to place detectors in strategic locations such as the upper ceiling of the enclosed area, the top section of the wall directly opposite the ventilation hole, above the air inlet, and atop the hydrogen tank.

4.3. Effect of Air Inlet and Ventilation Hole Locations on Ventilation Efficiency

Hydrogen, characterized by its low density and buoyancy, rapidly ascends to the ceiling when released at high velocities. Owing to this flow behavior, enhancing ventilation performance for leaked hydrogen requires adjustments in ventilation conditions. Vents in a ship are installed in fixed positions that cannot be changed for convenience. Therefore, if the locations of the vents are not considered during the ship design process, poor ventilation can lead to safety accidents. In other words, the locations of the vents can be a significant factor affecting ventilation efficiency.

Table 4 shows the parameters used to identify the characteristics based on the vent locations. The locations of the air inlets and exhaust vents presented in Table 4 are determined considering the physical and chemical properties of hydrogen as well as the airflow characteristics.

Table 4. Parameters for CFD investigation of effect of ventilation location.

Angle of Ceiling	Case	Leakage Rate (g/s)	Leakage Location	Inlet Position	Ventilation Position	Ventilation Velocity (m/s)	Temp (K)
120°	a	4	(0, 2.9, 2.0)	Inlet 1	Vent 1	2.73	298
	b	4	(0, 2.9, 2.0)	Inlet 1	Vent 2	2.73	298
	c	4	(0, 2.9, 2.0)	Inlet 2	Vent 1	2.73	298
	d	4	(0, 2.9, 2.0)	Inlet 2	Vent 2	2.73	298
	e	4	(0, 2.9, 2.0)	Inlet 3	Vent 1	2.73	298
	f	4	(0, 2.9, 2.0)	Inlet 3	Vent 2	2.73	298

To investigate the impact of ventilation port locations on hydrogen distribution—a key factor influencing ventilation efficiency—numerical simulations were conducted over a 600 s period based on the parametric setup outlined in Table 4.

Figure 5 depicts the ventilation system layout in the hydrogen tank storage room. In Figure 9a,c,e, the position of the ventilation hole was at Vent 1, while in Figure 9b,d,f, the position was at Vent 2. Among the configurations with different inlet positions (a), (c), and (e), the extent of hydrogen concentration exceeding 0.04 near the ceiling ranked as follows: (a) > (c) > (e). When measuring hydrogen concentrations of 0.04 or higher vertically downward from the point (0, 2.9, 2.0) near the ceiling, the distance from the ceiling was 0.83 m for (a), 0.75 m for (c), and undetectable for (e) except in some areas near the upper part of the hydrogen tank around the leak point.

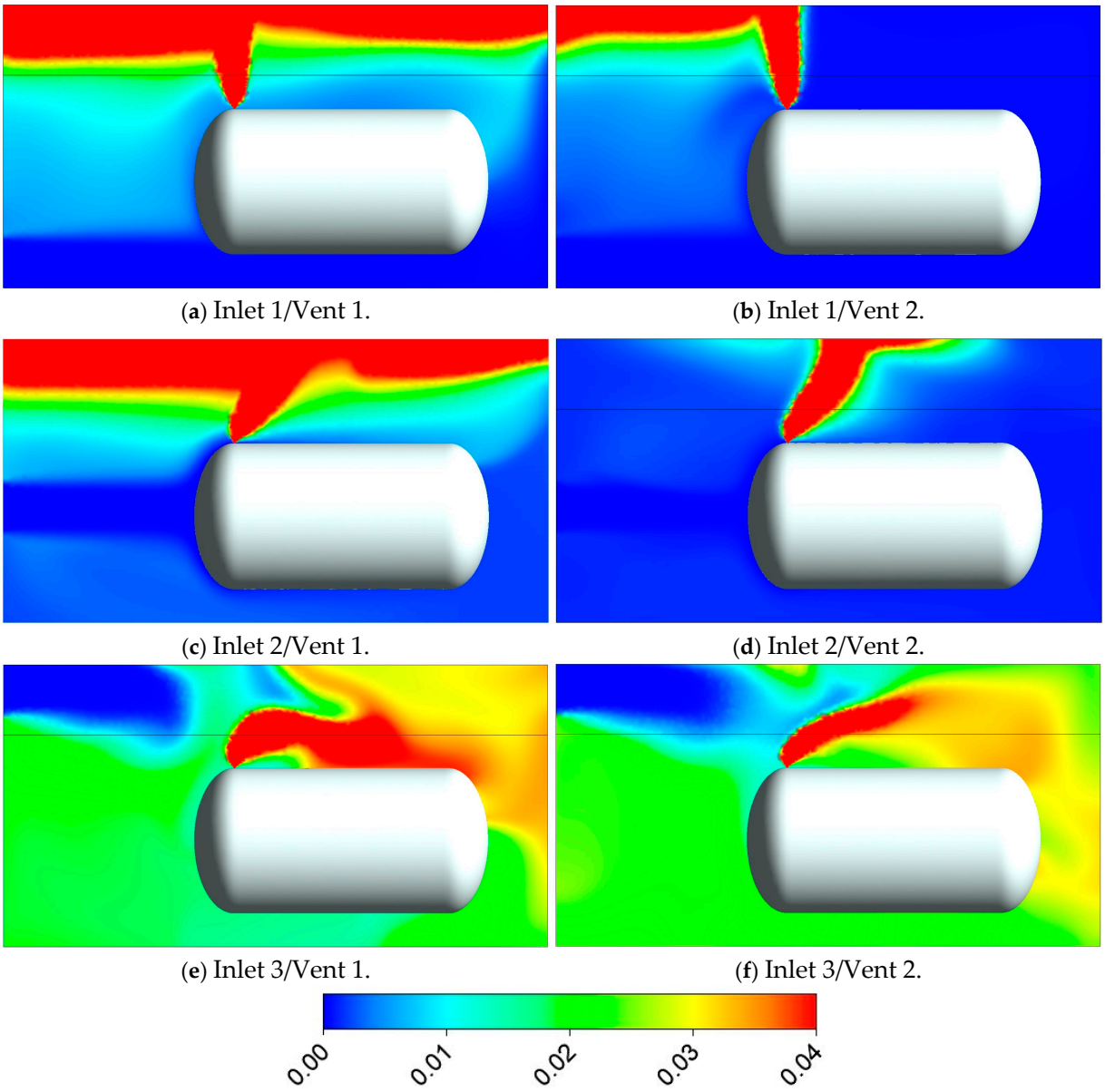


Figure 9. Hydrogen diffusion status according to the location of the ventilation hole.

Configurations (a) and (c) exhibited the most substantial hydrogen layer above the inlet wall, with concentrations decreasing toward the exhaust. However, in (e), owing to airflow from the inlet, the leaked hydrogen was directed toward the exhaust, resulting in hydrogen concentrations of 0.04 being limited to a small region above the hydrogen tank.

Configurations (b), (d), and (f) demonstrated lower overall ceiling concentrations compared to (a), (c), and (e). Notably, (d) showed almost no hydrogen stagnation near the ceiling, as hydrogen was exhausted through the ventilation hole located in the center of the ceiling (directly above the leak point), resulting in relatively efficient exhaust performance. In (b), the air inlet circulated beneath the hydrogen tank ascended along the ventilation wall and mixed with the leaked hydrogen, causing stagnation near the ceiling above the inlet wall. Configuration (f) displayed diffusion patterns similar to (e). These observations are consistent with the results presented in reference [53].

Comparing the six simulations, it can be concluded that to prevent the stagnation of leaked low-density hydrogen near the ceiling, the air inlet should be installed in the middle or upper part of the wall, and the ventilation hole should be placed on the ceiling above

the expected leak location. Additionally, installing the air inlet too low may lead to an expansion of the stagnation area near the ceiling.

Figure 10 illustrates the average hydrogen mole fraction over time within the hydrogen tank storage compartment. In the case of Vent 1 and Inlet 3, depicted in Figure 10a, the leaked hydrogen mixed with the air from the inlet, creating a zone of approximately 0.02 hydrogen concentration as it circulated through the storage area.

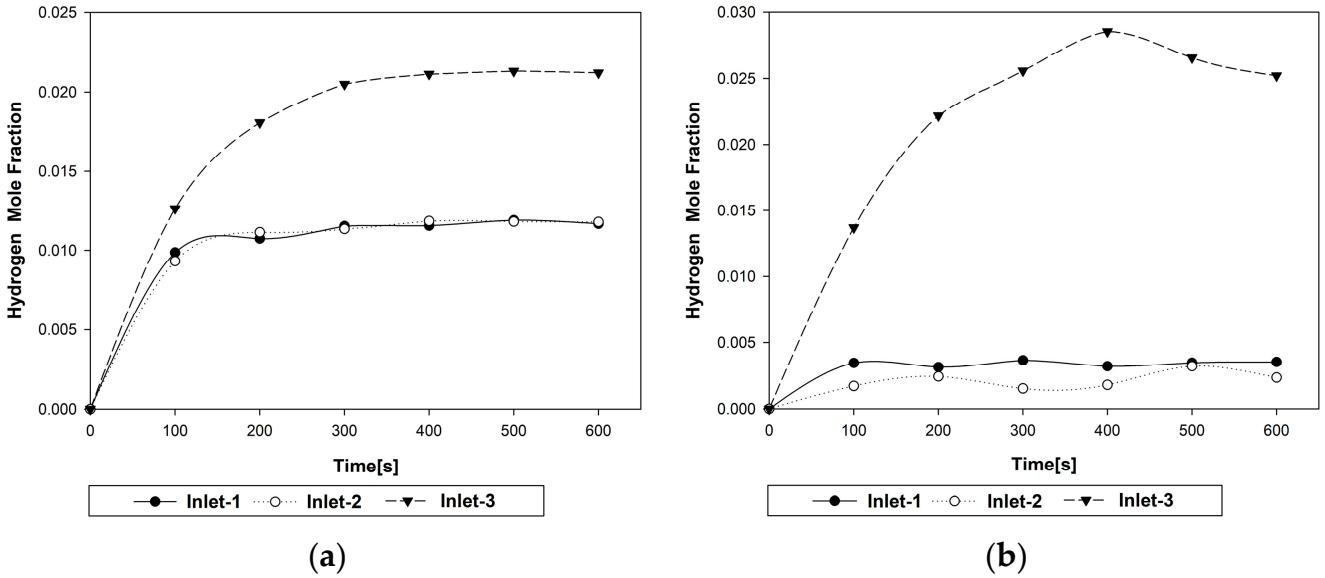


Figure 10. Average hydrogen mole fraction with changes in the positions of air inlets and ventilation holes (exhaust ports): (**a**) fixed Vent 1 and various air inlets, (**b**) fixed Vent 2 and various air inlets.

Inlet 3 is situated directly opposite the ventilation hole. The hydrogen mole fraction within the storage room maintained a steady level of about 0.02 from 300 s onwards, which is roughly twice the concentration observed with Inlet 1 and Inlet 2.

This result can be attributed to the air from Inlet 3 mixing with the leaked hydrogen and descending from the upper to the lower regions of the storage room, thereby enhancing the diffusion of the air–hydrogen mixture. Thus, when using a 4% hydrogen mole fraction as the flammability criterion, the Inlet 3 configuration may offer a marginally reduced risk at the ceiling level compared to Inlet 1 and Inlet 2, where leaked hydrogen tends to accumulate near the ceiling. However, this configuration could result in more extensive diffusion throughout the tank room.

Figure 10b indicates that the Vent 2 and Inlet 3 arrangement yielded the highest hydrogen concentration of 0.028 at 400 s, approximately 5.6 times greater than that observed with Inlet 1 and Inlet 2. Inlet 2 exhibited concentrations roughly half that of Inlet 1, and both were about five times lower than their counterparts in Figure 10a.

The results indicate that positioning the ventilation hole on the ceiling directly above the anticipated leak location proves more efficient than side-wall placement. Furthermore, locating the air inlet on the side-wall floor or at mid-wall height appears to yield superior ventilation outcomes.

4.4. Effect of Ventilation Velocity on Ventilation Efficiency

To examine how ventilation velocity influences ventilation in confined spaces, simulations were performed on scenarios exhibiting suboptimal ventilation conditions. The configurations (Inlet 1, Vent 1) and (Inlet 1, Vent 2) demonstrated high leaked hydrogen concentrations in the ceiling region, while (Inlet 3, Vent 1) and (Inlet 3, Vent 2) showed

the highest leaked hydrogen mole fractions in the storage room. These scenarios were numerically analyzed through simulations.

Ventilation velocities were set at 0, 1.82, 2.73, 3.64, 4.55, and 5.46 m/s, correlating to 0, 20, 30, 40, and 50 hourly air exchanges in the hydrogen tank storage room. Hydrogen diffusion patterns were evaluated 600 s after the leak. The findings are presented in Tables 5 and 6 and Figure 11. Table 5 presents isosurfaces of 4% hydrogen concentration at various exhaust velocities after 600 s, while Table 6 presents hydrogen concentration distributions in the YZ plane. Figure 11 depicts average hydrogen mole fractions in the storage room after 600 s.

Table 5. Flammable concentration isosurface (4%) with varying ventilation velocity at 600 s.

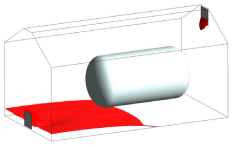
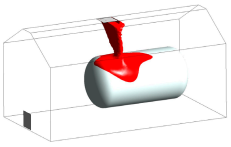
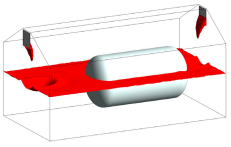
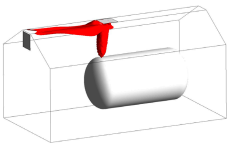
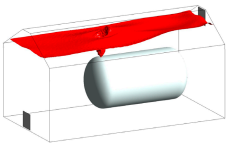
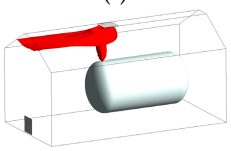
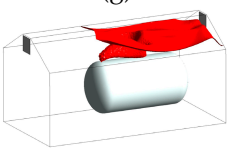
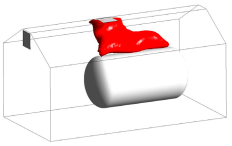
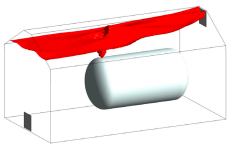
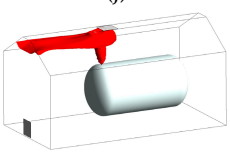
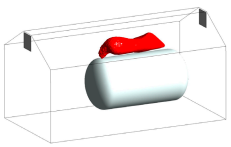
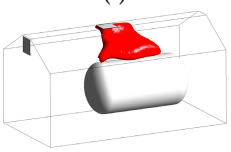
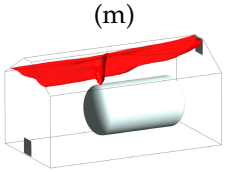
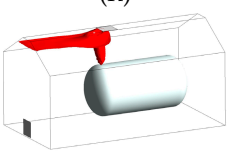
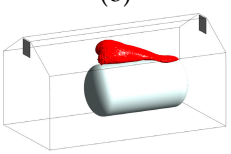
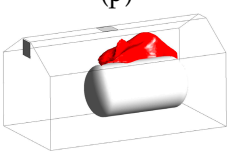
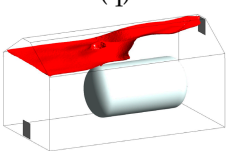
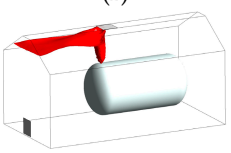
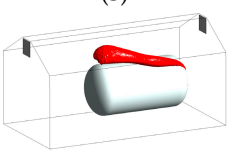
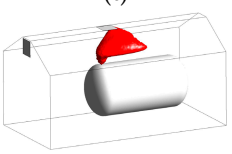
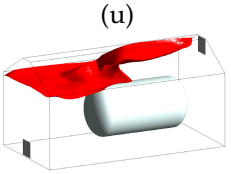
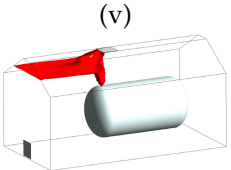
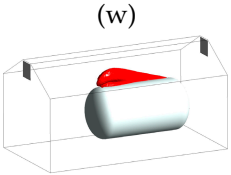
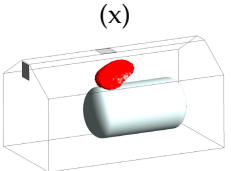
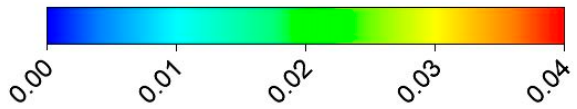
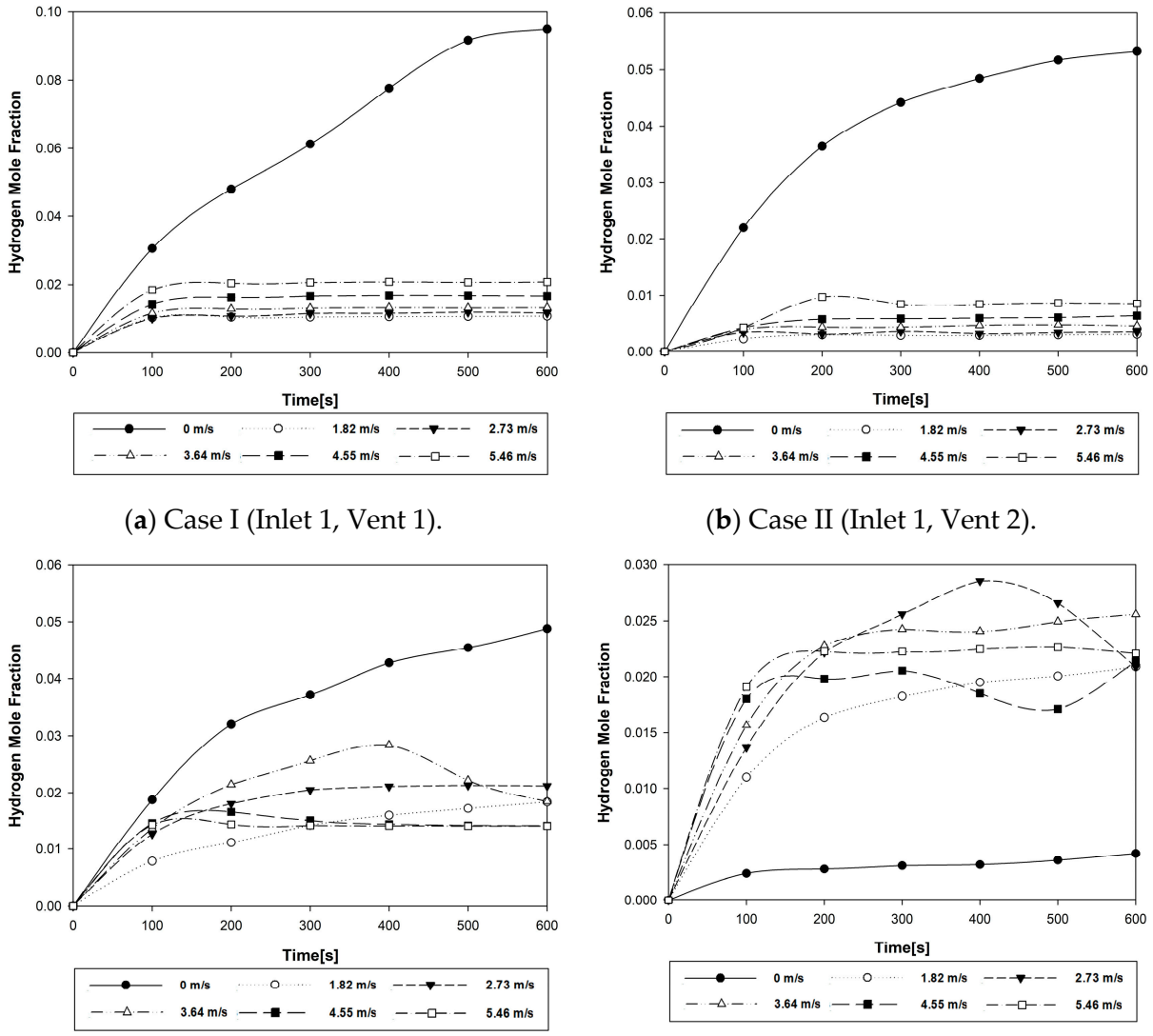
Ventilation Quantity (m/s)	Case			
	Inlet 1, Vent 1	**Inlet 1, Vent 2**	**Inlet 3, Vent 1**	**Inlet 3, Vent 2**
0	(a) 	(b) 	(c) 	(d) 
1.82	(e) 	(f) 	(g) 	(h) 
2.73	(i) 	(j) 	(k) 	(l) 
3.64	(m) 	(n) 	(o) 	(p) 
4.55	(q) 	(r) 	(s) 	(t) 
5.46	(u) 	(v) 	(w) 	(x) 

Table 6. H_2 concentration contours in the YZ plane.

Ventilation Quantity (m/s)	Case			
	Case I	**Case II**	**Case III**	**Case IV**
0	(a)	(b)	(c)	(d)
1.82	(e)	(f)	(g)	(h)
2.73	(i)	(j)	(k)	(l)
3.64	(m)	(n)	(o)	(p)
4.55	(q)	(r)	(s)	(t)
5.46	(u)	(v)	(w)	(x)



In Case I (a)–(u) of Table 5, the natural ventilation scenario (a) exhibited the highest hydrogen concentration, with a 4% concentration layer extending almost to the air inlet's center near the floor. For scenarios (e) and (i), as exhaust velocity increased, the leaked hydrogen formed stable layers near the ceiling except in proximity to the ventilation hole. In scenarios (m)–(u), as ventilation velocities increased, hydrogen concentrations notably decreased near the ventilation hole and dispersed from the ceiling toward the floor on the opposite side wall. This suggests that escalating exhaust velocities enhance hydrogen diffusion as it mixes with incoming air and follows the airflow patterns. The buoyant hydrogen did not simply stagnate in stable layers near the ceiling; rather, as ventilation velocity increased, the momentum of the incoming air from the inlet propelled the hydrogen to spread swiftly throughout the hydrogen tank storage room.



(**a**) Case I (Inlet 1, Vent 1).

(**b**) Case II (Inlet 1, Vent 2).

(**c**) Case III (Inlet 3, Vent 1).

(**d**) Case IV (Inlet 3, Vent 2).

Figure 11. Hydrogen mole fraction by ventilation.

In Case II (b)–(v) of Table 5, the 4% concentration regions were restricted to approximately half of the ceiling area directly above the leak source. This can be attributed to the ventilation hole's position directly above the leak point, which facilitated efficient hydrogen exhaust. Figure 11 demonstrates a roughly 50% improvement in ventilation efficiency compared to Case I. Under natural ventilation in scenario (b), the hydrogen's exit path through the ventilation hole was clearly identified. However, as presented in Table 6, Case II, increasing ventilation velocities caused the 4% concentration layer to gradually descend from the ceiling to the floor, similar to Case I, particularly near the side wall housing the air inlet.

In Case III (c)–(w) of Table 5, the 4% concentration zones were limited to the upper tank region extending from the leak point to the ventilation hole. When the air inlet was positioned opposite the ventilation hole, the incoming airflow effectively guided the leaked hydrogen toward the ventilation hole. Table 6, Case III, shows that increasing exhaust velocities resulted in the 4% concentration areas forming only in the immediate vicinity of the leak point, with generally diluted concentration layers throughout. The air influx from Inlet 3 appeared to disrupt hydrogen stagnation and accelerate the diffusion of low-concentration air–hydrogen mixtures, potentially mitigating flammable gas accumulation.

However, this effect is closely related to the ventilation hole's location, emphasizing the critical importance of air inlet positioning.

In Case IV (d)–(x) of Table 5, natural ventilation conditions (d) yielded the most limited 4% concentration zone. Table 6 indicates that leaked hydrogen was consistently evacuated through the ventilation hole situated above the leak point, largely unaffected by inlet airflow dynamics. Although increasing exhaust velocities progressively diminished the 4% concentration area, Figure 11d does not demonstrate a clear proportional relationship between exhaust velocity and ventilation efficacy. This observation suggests that optimal ventilation strategies must consider the relationship between air inlet and ventilation hole positions rather than relying solely on exhaust velocity.

Figure 11 illustrates that unlike in case (d), cases (a)–(c) exhibited peak hydrogen concentrations within the storage chamber under natural ventilation conditions. Optimal ventilation performance was achieved at a ventilation velocity of 1.82 m/s. Ventilation efficiency improved by approximately 50% when the ventilation hole was located directly above the leak source as opposed to side-wall placement. The Inlet 3 configuration, with the air inlet near the ceiling on the side wall, generated higher hydrogen concentrations compared to the Inlet 1 setup.

These observations suggest that increasing ventilation velocity corresponds with higher air inlet velocity, producing a dynamic conveyance effect. This disrupts the formation of stable hydrogen stratification at the ceiling level, promoting broader diffusion of the air–hydrogen mixture. This study concludes that while increasing ventilation velocity does not necessarily improve ventilation efficacy, achieving optimal ventilation efficiency requires a balanced consideration of air inlet and ventilation hole positions in conjunction with a suitable ventilation velocity.

When hydrogen leaks into a confined space, it undergoes diffusion and uniform mixing processes, with rapid leakage leading to simultaneous increases in hydrogen concentration and diffusion. As concentration differences gradually diminish, the confined space eventually reaches a uniform mixture of hydrogen and air, consistent with the results reported in reference [54]. Additionally, this study revealed that higher ventilation velocity further accelerates hydrogen diffusion, resulting in enhanced diffusion of the hydrogen–air mixture throughout the enclosed space.

5. Conclusions

This study conducted a numerical analysis of the flow and diffusion patterns of leaked hydrogen in confined environments, such as hydrogen tank storage compartments on ships. The simulation's accuracy for hydrogen diffusion behavior in enclosed spaces was validated by comparing the results with INERIS experimental data [50] and FDS simulations [51], confirming the reliability of the hydrogen flow characteristics model. The research examined how ceiling apex angle, leak rate, ventilation hole location, and ventilation velocity impact hydrogen diffusion and ventilation in confined spaces, yielding the following results:

(1) In enclosed areas such as ship interiors, hydrogen tank storage rooms typically have ceilings with specific apex angles. When hydrogen leaks in these confined spaces, it swiftly ascends to the ceiling owing to buoyancy, then gradually disperses and stratifies from ceiling to floor. A ceiling apex angle (A) of 177.7°, resembling a flat surface, produced thicker and more concentrated layers than a 120° angle. When A = 120°, thinner hydrogen concentration layers were generated than at 177.7°, even under natural ventilation conditions. The result suggests that the ceiling apex angle significantly affects ventilation efficacy and should be a key consideration in designing efficient ventilation systems.

(2) Increased leak rates resulted in sustained hydrogen concentration growth within the storage room, and the diffusion characteristics exhibited similar trends. Upon leakage, hydrogen rises to the ceiling, flows along its surface, gradually stratifies, partially exhausts, and the remaining portion mixes with inlet air to circulate throughout the storage room. The upper vertical section of the side wall with the air inlet developed higher hydrogen concentration layers compared to the side wall with the ventilation hole. Based on these flow dynamics, hydrogen leak detectors should be installed on the upper section of the side wall directly opposite the ventilation hole, on the upper part of the side wall with the air inlet, and above the hydrogen tank.

(3) To rapidly exhaust leaked hydrogen, careful consideration of air inlet and ventilation hole positions is essential. Ventilation holes located on the ceiling directly above the leak source demonstrated superior ventilation performance compared to side-wall installations. Air inlets positioned on the side-wall floor or at mid-wall height exhibited enhanced ventilation effects compared to locations near the ceiling.

(4) Escalating ventilation velocity led to increased air inlet velocity. The dynamic transport effect of the air inlet disrupted hydrogen stratification at the ceiling level, resulting in expanded diffusion of the air–hydrogen mixture. Optimal ventilation effects were generally observed at 1.82 m/s, equivalent to 20 air changes per hour. However, increasing ventilation velocity does not necessarily improve ventilation effectiveness. Therefore, the configuration of air inlets and ventilation holes must be optimized simultaneously. Otherwise, it may result in accelerated hydrogen diffusion owing to the increased ventilation velocity.

In future studies, the impact of structures installed on the ceiling of the hydrogen tank storage room and the effect of ship motions such as rolling and pitching on ventilation efficiency will be analyzed. The analyzing factors affecting ventilation are crucial for ensuring the safety of hydrogen ships isolated at sea. Additionally, it is essential to reduce the fatal damage to human life, ships, and cargo caused by any hydrogen fires.

Author Contributions: Conceptualization, C.-Y.L. and S.-K.P.; methodology, C.-Y.L. and S.-K.P.; software, C.-Y.L.; validation, C.-Y.L. and S.-K.P.; formal analysis, S.-K.P.; writing—original draft preparation, C.-Y.L. and S.-K.P.; writing—review and editing, C.-Y.L. and S.-K.P.; visualization, C.-Y.L.; supervision, S.-K.P.; funding acquisition, S.-K.P. All authors have read and agreed to the published version of the manuscript.

Funding: This research received no funding.

Data Availability Statement: The original contributions presented in the study are included in the article, further inquiries can be directed to the corresponding author.

Conflicts of Interest: The authors have no conflicts of interest to declare.

References

1. Ishaq, H.; Dincer, I.; Crawford, C. A review on hydrogen production and utilization: Challenges and opportunities. *Int. J. Hydrogen Energy* **2022**, *47*, 26238–26264. [CrossRef]
2. Kanna, V.; Roseline, S.; Balalmurugan, K.; Jeeva, S.; Santhiyagu, I.A. The Effects of Greenhouse Gas Emissions on Global Warming, Encyclopedia of Renewable Energy. *Sustain. Environ.* **2024**, *1*, 143–154.
3. United Nations (UN). The key outcomes of COP28. In Proceedings of the UN Climate Change Conference, Dubai, United Arab Emirates, 30 November–12 December 2023.
4. Wang, Z.; Zhao, F.; Dong, B.; Wang, D.; Ji, Y.; Cai, W.; Han, F. Life cycle framework construction and quantitative assessment for the hydrogen fuelled ships: A case study. *Ocean. Eng.* **2023**, *281*, 114740. [CrossRef]
5. IMO. Annex 9. Resolution MEPC.213(63). Adopted on 2 March 2012. 2012 Guidelines for the Development of a Ship Energy Efficiency Management Plan. Available online: https://wwwcdn.imo.org/localresources/en/KnowledgeCentre/IndexofIMOResolutions/MEPCDocuments/MEPC.213(63).pdf (accessed on 14 June 2024).

6. IMO. Fourth IMO GHG Study 2020. Available online: https://www.imo.org/en/ourwork/Environment/Pages/Fourth-IMO-Greenhouse-Gas-Study-2020.aspx (accessed on 17 June 2024).
7. IMO. 2023 IMO Strategy on Reduction of GHG Emissions from Ships MEPC.377(80). Available online: https://www.imo.org/en/OurWork/Environment/Pages/2023-IMO-Strategy-on-Reduction-of-GHG-Emissions-from-Ships.aspx (accessed on 19 June 2024).
8. Wang, Y.; Cao, Q.; Liu, L.; Wu, Y.; Liu, H.; Gu, Z.; Zhu, C. A review of low and zero carbon fuel technologies: Achieving ship carbon reduction targets. *Sustain. Energy Technol. Assess.* **2022**, *54*, 102762. [CrossRef]
9. American Bureau of Shipping (ABS). Setting the Course to Low Carbon Shipping. Available online: https://ww2.eagle.org/content/dam/eagle/advisories-and-debriefs/low-carbon-shipping-outlook-2019.pdf (accessed on 20 June 2024).
10. DNV GL. Assessment of Selected Alternative Fuels and Technologies. Available online: https://www.dnv.com/maritime/publications/alternative-fuel-assessment-download/ (accessed on 22 June 2024).
11. DNV GL. Maritime Forecast to 2050. Energy Transition Outlook 2019. Available online: https://sustainableworldports.org/wp-content/uploads/DNV-GL_2019_Maritime-forecast-to-2050-Energy-transition-Outlook-2019-report.pdf (accessed on 22 June 2024).
12. Ampah, J.D.; Yusuf, A.A.; Afrane, S.; Jin, C.; Liu, H. Reviewing two decades of cleaner alternative marine fuels: Towards IMO's decarbonization of the maritime transport sector. *J. Clean. Prod.* **2021**, *320*, 128871. [CrossRef]
13. Mukherjee, A.; Bruijnincx, P.; Junginger, M. Techno-economic competitiveness of renewable fuel alternatives in the marine sector. *Renew. Sustain. Energy Rev.* **2023**, *174*, 113127. [CrossRef]
14. Wang, Z.; Dong, B.; Yin, J.; Li, M.; Ji, Y.; Han, F. Towards a marine green power system architecture: Integrating hydrogen and ammonia as zero-carbon fuels for sustainable shipping. *Int. J. Hydrogen Energy* **2024**, *50*, 1069–1087. [CrossRef]
15. Wu, Y.; Chen, A.; Xiao, H.; Jano-lto, M.; Alnaeli, M.; Alnajideen, M.; Mashruk, S.; Valera-Medina, A. Emission reduction and cost-benefit analysis of the use of ammonia and green hydrogen as fuel for marine applications. *Green. Energy Resour.* **2023**, *1*, 100046. [CrossRef]
16. Machaj, K.; Kupecki, J.; Malecha, Z.; Morawski, A.W.; Skrzypkiewicz, M.; Stanclik, M.; Chorowski, M. Ammonia as a potential marine fuel: A review. *Energy Strategy Rev.* **2024**, *55*, 101504. [CrossRef]
17. Jang, H.; Mujeeb-Ahmed, M.P.; Wang, H.; Park, C.; Hwang, I.; Jeong, B.; Zhou, P.; Mickeviciene, R. Regulatory gap analysis for risk assessment of ammonia-fuelled ships. *Ocean. Eng.* **2023**, *287*, 115751. [CrossRef]
18. Inal, O.B.; Zincir, B.; Deniz, C. Investigation on the decarbonization of shipping: An approach to hydrogen and ammonia. *Int. J. Hydrogen Energy* **2022**, *47*, 19888–19900. [CrossRef]
19. Morlanés, N.; Katikaneni, S.P.; Paglieri, S.N.; Harale, A.; Solami, B.; Sarathy, S.M.; Gascon, J. A technological roadmap to the ammonia energy economy: Current state and missing technologies. *Chem. Eng. J.* **2021**, *408*, 127310. [CrossRef]
20. Zincir, B. Environmental and economic evaluation of ammonia as a fuel for short-sea shipping: A case study. *Int. J. Hydrogen Energy* **2022**, *47*, 18148–18168. [CrossRef]
21. Xing, H.; Stuart, C.; Spence, S.; Chen, H. Alternative fuel options for low carbon maritime transportation: Pathways to 2050. *J. Clean. Prod.* **2021**, *297*, 126651. [CrossRef]
22. Erdemir, D.; Dincer, I. A perspective on the use of ammonia as a clean fuel: Challenges and solutions. *Int. J. Energy Res.* **2020**, *45*, 4827–4834. [CrossRef]
23. Yang, F.; Wang, T.; Deng, X.; Dang, J.; Huang, Z.; Hu, S.; Li, Y.; Ouyang, M. Review on hydrogen safety issues: Incident statistics, hydrogen diffusion, and detonation process. *Int. J. Hydrogen Energy* **2021**, *46*, 31467–31488. [CrossRef]
24. Yang, Z.; Hao, D.; Wang, F.; Qin, C.; Chen, X.; Tian, Y. Quantitative analysis of hydrogen leakage and diffusion processes based on real-time concentration measurement at different spatial positions in a customized chamber. *Int. J. Hydrogen Energy* **2024**, *66*, 231–241. [CrossRef]
25. Li, H.; Cao, X.; Shao, Y.; Nan, Z.; Teng, L.; Peng, W.; Bian, J. Safety of hydrogen storage and transportation: An overview on mechanisms, techniques, and challenges. *Energy Rep.* **2022**, *8*, 6258–6269. [CrossRef]
26. Saffers, J.B.; Molkov, V.V. Hydrogen safety engineering framework and elementary design safety tools. *Int. J. Hydrogen Energy* **2014**, *39*, 6268–6285. [CrossRef]
27. Abohamzeh, E.; Salehi, F.; Sheikholeslami, M.; Abbassi, R.; Khan, F. Review of hydrogen safety during storage, transmission, and applications processes. *J. Loss Prev. Process Ind.* **2021**, *72*, 104569. [CrossRef]
28. Li, X.; Hao, Y.; Wu, F.; Xing, Z.; Zhuang, S.; Wang, X. Numerical simulation of leakage jet flame hazard of high-pressure hydrogen storage bottle in open space. *Int. J. Hydrogen Energy* **2024**, *62*, 706–721. [CrossRef]
29. Lyu, S.; Huang, X.; Peng, S.; Sun, M.; Qi, Q.; Aimaieraili, D. A novel method for analyzing the leakage and diffusion of hydrogen: First arrival time distribution. *Renew. Sustain. Energy Rev.* **2024**, *198*, 114451. [CrossRef]
30. Xin, J.; Duan, Q.; Jin, K.; Sun, J. A reduced-scale experimental study of dispersion characteristics of hydrogen leakage in an underground parking garage. *Int. J. Hydrogen Energy* **2023**, *48*, 16936–16948. [CrossRef]

31. Shu, Z.; Liang, W.; Zheng, X.; Lei, G.; Cao, P.; Dai, W.; Qian, H. Dispersion characteristics of hydrogen leakage: Comparing the prediction model with the experiment. *Energy* **2021**, *236*, 12420. [CrossRef]
32. Hussein, H.; Brennan, S.; Molkov, V. Dispersion of hydrogen release in a naturally ventilated covered car park. *Int. J. Hydrogen Energy* **2020**, *45*, 23882–23897. [CrossRef]
33. Schiavetti, M.; Carcassi, M.N. Experimental tests of inhomogeneous hydrogen deflagrations in the presence of obstacles. *Int. J. Hydrogen Energy* **2021**, *46*, 12455–12463. [CrossRef]
34. Kuznetsov, M.; Friedrich, A.; Stern, G.; Kotchourko, N.; Jallais, S.; L'Hostis, B. Medium-scale experiments on vented hydrogen deflagration. *J. Loss Prev. Process Ind.* **2015**, *36*, 416–428. [CrossRef]
35. Li, Y.; Zhao, Z.; Qi, W.; Yao, Z.; Wang, J.; Ding, Z.; Lv, H. Accuracy analysis of hydrogen leakage scale modeling based on similarity theory. *Int. J. Hydrogen Energy* **2024**, *68*, 537–544. [CrossRef]
36. Zhang, W.; Liu, M.; Xiao, Y.; Wu, Q.; Wang, J.; Wang, T.; Zhang, Y. Numerical study of hydrogen leakage dispersion and explosion of a 2 × 120 kW PEM fuel cell integrated power station. *Int. J. Hydrogen Energy* **2024**. [CrossRef]
37. Tian, Y.; Qin, C.; Yang, Z.; Hao, D. Numerical simulation study on the leakage and diffusion characteristics of high-pressure hydrogen gas in different spatial scenes. *Int. J. Hydrogen Energy* **2024**, *50*, 1335–1349. [CrossRef]
38. Lv, H.; Shen, Y.; Zheng, T.; Zhou, W.; Ming, P.; Zhang, C. Numerical study of hydrogen leakage, diffusion, and combustion in an outdoor parking space under different parking configurations. *Renew. Sustain. Energy Rev.* **2023**, *173*, 113039. [CrossRef]
39. Abbas, M.A.H.; Kheradmand, S.; Sadoughipour, H. Numerical study of the effect of hydrogen leakage position and direction on hydrogen distribution in a closed enclosure. *Int. J. Hydrogen Energy* **2020**, *45*, 23872–23881. [CrossRef]
40. Qian, J.Y.; Li, X.J.; Gao, Z.X.; Jin, Z.J. A numerical study of hydrogen leakage and diffusion in a hydrogen refueling station. *Int. J. Hydrogen Energy* **2020**, *45*, 14428–14439. [CrossRef]
41. Li, F.; Yuan, Y.; Yan, X.; Malekian, R.; Li, Z. A study on a numerical simulation of the leakage and diffusion of hydrogen in a fuel cell ship. *Renew. Sustain. Energy Rev.* **2018**, *97*, 177–185. [CrossRef]
42. Gao, Y.; Liu, H.; Hou, Y. Effects of leakage location and ventilation condition on hydrogen leakage during shipping of fuel cell vehicles. *Int. J. Hydrogen Energy* **2024**, *54*, 1532–1543. [CrossRef]
43. Mao, X.; Ying, R.; Yuan, Y.; Li, F.; Shen, B. Simulation and analysis of hydrogen leakage and explosion behaviors in various compartments on a hydrogen fuel cell ship. *Int. J. Hydrogen Energy* **2021**, *46*, 6857–6872. [CrossRef]
44. Xie, Y.; Liu, J.; Qin, J.; Xu, Z.; Zhu, J.; Liu, G.; Yuan, H. Numerical simulation of hydrogen leakage and diffusion in a ship engine room. *Int. J. Hydrogen Energy* **2024**, *55*, 42–54. [CrossRef]
45. Kim, B.; Hwang, K. Effect of angular motion on accidental hydrogen fires in conceptional ship fuel preparation room with mechanical ventilation. *Int. J. Hydrogen Energy* **2024**, *50*, 1075–1090. [CrossRef]
46. Kim, B.; Hwang, K. Experimental analysis of the effects of ship motion on hydrogen dispersion in an enclosed area. *Int. J. Hydrogen Energy* **2023**, *48*, 31779–31789. [CrossRef]
47. Soto, V.; Baalisampang, T.; Arzaghi, E.; Garaniya, V. Numerical modelling of hydrogen release and dispersion in under-deck compressed hydrogen storage of marine ships. *Int. J. Hydrogen Energy* **2024**, *59*, 1244–1256. [CrossRef]
48. ANSYS, Inc. *ANSYS CFX Solver Theory Guide*, 18th ed.; ANSYS, Inc.: Canonsburg, PA, USA, 2017.
49. Li, H.; Cao, X.; Du, H.; Teng, L.; Shao, Y.; Bian, J. Numerical simulation of leakage and diffusion distribution of natural gas and hydrogen mixtures in a closed container. *Int. J. Hydrogen Energy* **2022**, *47*, 35928–35939. [CrossRef]
50. Lacome, J.M.; Jamois, D.; Perrette, L.; Proust, C.H. Large-scale hydrogen release in an isothermal confined area. *Int. J. Hydrogen Energy* **2011**, *36*, 2302–2312. [CrossRef]
51. Zhang, Z.; Delichatsios, M.A.; Venetsanos, A.G. Numerical studies of dispersion and flammable volume of hydrogen in enclosures. *Int. J. Hydrogen Energy* **2010**, *35*, 6431–6437. [CrossRef]
52. Hajji, Y.; Bouteraa, M.; Cafsi, A.E.; Belghith, A.; Bournot, P.; Kallel, F. Dispersion and behavoir of hydrogen during a leak in a prismatic cavity. *Int. J. Hydrogen Energy* **2014**, *39*, 6111–6119. [CrossRef]
53. Patel, P.; Baalisampang, T.; Arzaghi, E.; Garaniya, V.; Abbassi, R.; Salehi, F. Computational analysis of the hydrogen dispersion in semi-confined spaces. *Process Saf. Environ. Prot.* **2023**, *176*, 475–488. [CrossRef]
54. Kang, Y.; Ma, S.; Song, B.; Xia, X.; Wu, Z.; Zhang, X.; Zhao, M. Simulation of hydrogen leakage diffusion behavior in confined space. *Int. J. Hydrogen Energy* **2024**, *53*, 75–85. [CrossRef]

Disclaimer/Publisher's Note: The statements, opinions and data contained in all publications are solely those of the individual author(s) and contributor(s) and not of MDPI and/or the editor(s). MDPI and/or the editor(s) disclaim responsibility for any injury to people or property resulting from any ideas, methods, instructions or products referred to in the content.